Project 6: Catastrophe Optics

Gianfranco Grillo

December 1st, 2017

Abstract

We propose a simple experiment designed to explore the far field diffraction pattern of a water droplet, and show the results of simulations based on a simple model for the water droplet shape, which are in line with results from previous experiments. Liquid droplets can act as imperfect lenses, and give rise to interesting near and far field diffraction patterns that contain caustics, which correspond to envelopes of light rays projected onto a surface. At the caustics, the geometrical optics approximation breaks down, and a proper description of the intensity patterns needs to be obtained via a more sophisticated mathematical treatment based on catastrophe theory. Different types of caustics can be obtained depending on the number of control parameters that are part of a generating function. These control parameters can be identified with experimental variables that can be altered during the course of an experiment.

1 Introduction

A very useful way to describe the propagation of light is to model it as rays whose direction is determined by the nature of the medium on which the light is propagating. Propagation through certain types of physical structures often result in the rays converging towards a specific area in space. In the idealized picture, rays of light parallel to the optical axis that are incident on a beam with focal length f will focus at a single point in the optical axis at a distance f away from the lens. In reality, however, this picture is inaccurate. Conservation of energy implies that the intensity of the light at the focal point would be infinite, since the area of the point is zero, which is not physically possible. This unphysical situation is never substantiated because lenses always suffer from some degree of aberration. This means that instead of coming into focus at a point, light comes into focus at a caustic surface in space that has non-zero area. Furthermore, the geometrical optics point of view ignores diffraction effects, which also affect the intensity of the light at the focus. The study of aberrations and their effects is an important area of optics, especially because of the practical implications they have for the proper construction of optical systems. However, the picture of an aberrated lens is not very useful for describing the irradiance patterns that arise from the lensing of light by manifestly imperfect structures such as liquid droplets. Instead, a different approach, based on the catastrophe theory of mathematicians Rene Thom (Thom 1972) and Vladimir Arnol'd (Arnol'd 1975), and applied to optics by Sir Michael Berry and others (Berry 1976, Berry & Upstill 1980, Nye 1978), has been very successful in describing the general characteristics of the extremely complex intensity patterns that can be observed when light is incident on transparent materials with irregular shapes. Catastrophe optics has also proven useful in analyzing the intensity patterns of astrophysical sources (Clegg et al. 1998, Cordes et al. 2017).

The goal of the experiment proposed in this project is to be able to observe the different types of caustics that can be produced in the far field irradiance pattern of light incident on a small water droplet, and compare the structure of these caustics to that predicted by catastrophe optics.

2 Theoretical background

2.1 Lensing geometry in the geometrical optics approximation

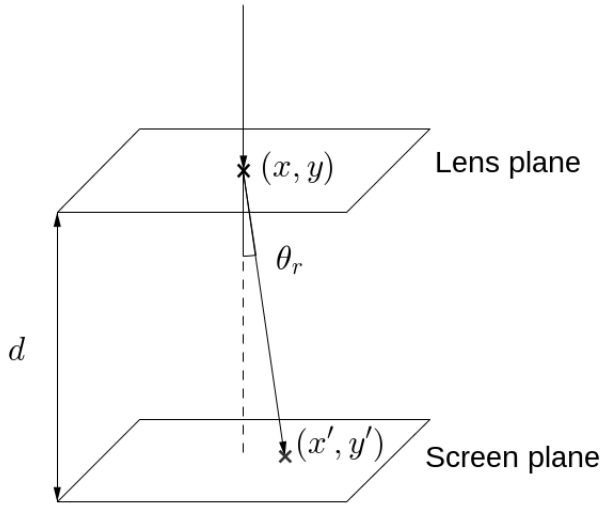

Figure 1: Lensing geometry.

In the geometrical optics approximation, the propagation of light is described in terms of rays, and the possible manifestations of the wave nature of light such as diffraction are ignored by considering the limit of zero wavelength, $\lambda \to 0$. This approximation is extremely useful in practice because of the simple propagation picture that it entails, and because the visible wavelength of electromagnetic waves is very small. In this framework, it is possible to visualize what happens when light traveling through one medium is incident upon a transparent structure, or lens, by thinking about it in terms of how the constituent rays deviate from their original trajectory. Let a beam of collimated light be normally incident on the lens. Then if we consider a single ray that strikes the structure at a point $\vec{x} = \begin{bmatrix} x \\ y \end{bmatrix}$ in the lens's plane, it will emerge at the other side having been refracted by a certain angle $\vec{\theta_r} = \begin{bmatrix} \theta_x \\ \theta_y \end{bmatrix}$, which will depend on the wavelength of the light, the lens material, the lens shape, and the nature of the surrounding medium. If we now place a screen at distance d from the lens plane, the refracted ray will arrive at the screen at a second set of coordinates on the screen plane, $\vec{x}' = \begin{bmatrix} x' \\ y' \end{bmatrix}$. Since we are interested in the far field, we can assume d to be large with respect to the path difference, so the angle to be small, which implies that the relationship between the two sets of coordinates in the

lens and the screen plane will be given by

$$\vec{x}' = \vec{x} - d\vec{\theta}_r \tag{1}$$

which is known as the lens equation.

Following Clegg et. al. (1998), a general expression for the refractive angle can be obtained in the geometrical optics limit with the additional assumptions that the lens's surface slope is small, and the lens's medium is uniform. The result of the ray propagating through the lens is that the lens advances or retards the ray's phase, depending on whether the value of the refractive index is greater or smaller than unity, because the phase velocity will be greater or smaller than the speed of light. More precisely, we can write the phase difference $\delta\phi_{lens}$ as

$$\delta\phi = \omega\tau = kc\tau \tag{2}$$

where τ is the propagation time difference between an unlensed ray and a lensed ray and $k = \frac{2\pi}{\lambda}$ is the wavenumber. For a rectangular lens of length l parallel to the direction of propagation, this is

$$\tau = \frac{l}{c}(1-n) \tag{3}$$

If we let the lens shape in the propagation direction be an arbitrary function of x and y, $f(\vec{x})$, we can then write (2) as

$$\delta\phi_{lens} = kf(\vec{x})(1-n) \tag{4}$$

According to geometrical optics, rays propagate in the direction normal to the surfaces of constant phase (Born & Wolf 1999, chapter III). What this implies is that the shape of the wavefront emerging from the lens will depend on $f(\vec{x})$, and$\vec{\theta}_r$ can be written as

$$\begin{aligned}\vec{\theta}_r &= \frac{1}{k}\nabla\delta\phi_{lens} \\ &= (1-n)\nabla f(\vec{x})\end{aligned} \tag{5}$$

Where we have assumed that $d \gg f(\vec{x})$. The lens equation (1) then becomes

$$\vec{x}' = \vec{x} + d(n-1)\nabla f(\vec{x}) \tag{6}$$

We now define a lens scale a that characterizes the size of the lens, and define the dimensionless quantities $\vec{u}' = \frac{\vec{x}'}{a}$, $\vec{u} = \frac{\vec{x}}{a}$, and rewrite $f(\vec{x})$ as $hf(\vec{u})$, where h is the maximum height of the lens above the lens plane, and $f(\vec{u})$ is a dimensionless function with unit maximum. This gives

$$\vec{u}' = \vec{u} + \frac{dh(n-1)}{a^2}\nabla_{\vec{u}} f(\vec{u}) \tag{7}$$

Finally, we define dimensionless quantities $H = \frac{h}{a}$ and $D = \frac{d}{a}$, and write

$$\vec{u}' = \vec{u} + DH(n-1)\nabla_{\vec{u}} f(\vec{u}) \tag{8}$$

An important property of this equation, which is simply a mapping from the lens plane to the screen plane, is that depending on the nature of the lens shape function $f(\vec{u})$, and the values of n, a, d, and h, more than one solution may exist for a given coordinate in the screen plane. This means that an observer at certain coordinates in the screen plane can potentially observe more than one image of the light that is incident on the lens. The points at which these images merge play a central role in catastrophe optics.

2.2 Geometrical optics intensity

The lens will have a focusing or defocusing effect on the rays that are incident on it. The magnification, or gain, of the lens is a measure of the focusing and defocusing of the rays at a certain point on the screen. With this in mind, we can define a Hessian matrix $[H]$ given by (Thorne & Blandford 2017, chapter 7),

$$[H] = \begin{bmatrix} \frac{\partial u_x}{\partial u'_x} & \frac{\partial u_y}{\partial u'_x} \\ \frac{\partial u_x}{\partial u'_y} & \frac{\partial u_y}{\partial u'_y} \end{bmatrix} \tag{9}$$

$$= \begin{bmatrix} 1 + DH(n+1)\partial^2_{u_x} f(\vec{u}) & DH(n+1)\partial_{u_x u_y} f(\vec{u}) \\ DH(n+1)\partial_{u_x u_y} f(\vec{u}) & 1 + DH(n+1)\partial^2_{u_y} f(\vec{u}) \end{bmatrix} \tag{10}$$

For a given solution of the lens equation $\vec{u}_k$, the gain G is then given by the reciprocal of the absolute value of the determinant of the Hessian matrix, ie.

$$G = \left| \left(1 + DH(n+1)\partial^2_{u_x} f(\vec{u})\right) \left(1 + DH(n+1)\partial^2_{u_y} f(\vec{u})\right) - \left(DH(n+1)\partial_{u_x u_y} f(\vec{u})\right)^2 \right|^{-1}_{\vec{u}=\vec{u}_k} \tag{11}$$

It is immediately apparent from the form of this equation that the gain diverges at certain values of $\vec{u}_k$ for a given set of parameters d, h, a, and n. These correspond to locations in which the determinant of H vanishes, and determine caustic locations. Geometrical optics fails at these locations, as it predicts an infinite intensity. We call these locations catastrophes. As mentioned before, the number of solutions to the lens equation changes at either side of a caustic, as multiple images merge at the caustic location. The number of images that merge determine the behavior of the intensity pattern at and near the caustic.

2.3 The classification of catastrophes

Name	Standard polynomial
Fold	$\frac{1}{3}u_x^3 + u_x u'_x$
Cusp	$\frac{1}{4}u_x^4 + \frac{1}{2}u_x^2 u'_x + u_x u'_y$
Swallowtail	$\frac{1}{5}u_x^5 + \frac{1}{3}Du_x^3 + \frac{1}{2}u_x^2 u'_y + u_x u'_x$
Elliptic umbilic	$u_x^3 - 3u_x u_y^2 - D(u_x^2 + u_y^2) - u_x u'_x - u_y u'_y$
Hyperbolic umbilic	$u_x^3 + u_y^3 + Du_x u_y - u_x u'_x - u_y u'_y$

Table 1: Names and standard polynomials for the first five elementary catastrophes.

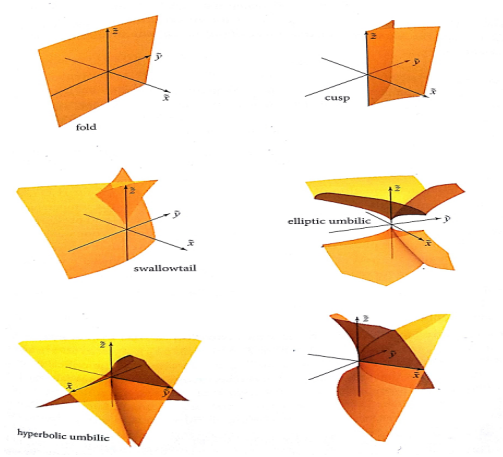

Figure 2: Surfaces of the elementary catastrophes. Note that the notation is different to the one used in this work. They are related by $\tilde{x} = u_x$, $\tilde{y} = u_y$, and $\tilde{z} = D$. Adapted from Thorne & Blandford (2017).

Since geometrical optics fails at catastrophe locations, it is necessary to apply wave optics in order to describe the intensity pattern near the caustics. In the far field regime, the scalar field ϵ is given by the Kirchoff's diffraction integral,

$$\epsilon(\vec{u}') = \frac{1}{2\pi u_F^2} \iint du_x\, du_y \exp\left[\imath\delta\phi\right] \tag{12}$$

where u_F corresponds to the normalized Fresnel scale, given by

$$u_F = \frac{1}{a}\sqrt{\frac{d}{k}} \tag{13}$$

The phase difference $\delta\phi$ between a refracted ray and an unrefracted one can be written in terms of the geometrical phase difference $\delta\phi_{geo}$ and the phase change introduced by the lens $\delta\phi_{lens}$

$$\begin{aligned}\delta\phi &= \delta\phi_{geo} + \delta\phi_{lens} \\ &= \frac{ka^2}{2d}\left|\vec{u}' - \vec{u}\right|^2 + kh(1-n)f(\vec{u}) \\ &= \frac{\left|\vec{u}' - \vec{u}\right|^2}{2u_F^2} + kh(1-n)f(\vec{u})\end{aligned} \tag{14}$$

The geometrical optics gain can be obtained by solving (12) using the method of stationary phase (Born & Wolf 1999, appendix III), and then taking the squared magnitude of the result for each of the

stationary phase solutions, which correspond to the gain for each of the images that are observable at the screen. As noted before, however, this method fails close to caustics, which correspond to the locations in which a number of images merge. Near the caustics, and depending on the number of images at each side, we can write $\delta\phi$ in terms of a standard polynomial that describes the behavior of the phase at or near the caustic. In 3D, there exist five possible types of catastrophes, each described by a different standard polynomial. These are the fold, cusp, swallowtail, elliptic umbilic, and hyperbolic umbilic. A graphical representation is given in Figure 2, and the standard polynomials for each of the catastrophes are given in Table 1. What is important to note is that the standard polynomials of higher order catastrophes have a larger number of parameters than the ones in lower order catastrophes. This means that depending on the number of parameters that can be altered in an experimental setup, it is possible to observe some catastrophes but not others. In the present context, the screen coordinates constitute two control parameters that potentially enable us to observe fold and cusp catastrophes depending on the shape that the water droplet adopts, but in order to observe higher order catastrophes it is necessary to also alter the distance d between the screen and the lens. It is in principle possible to observe higher order catastrophes if one introduces another control parameter in the experiment, such as by holding the lens at an angle with respect to the xy-plane, but we will not explore this possibility in the present project.

2.4 Liquid droplet structure

Following the approach in Berry (1976) and Nye (1978), a liquid droplet with characteristic radius $a < 1.5$ mm that is placed on a flat horizontal surface will not have its shape noticeably altered by gravity, and we can regard its internal pressure p as constant. The elevation above the lens plane $f(\vec{x})$ will then be constrained by the equation

$$\nabla^2 f = -\frac{p}{\gamma} \tag{15}$$

where γ is the surface tension of the liquid. We can rewrite this in dimensionless coordinates using the already introduced variables h and a, as

$$\nabla_{\vec{u}} f(\vec{u}) = -\frac{pa^2}{\gamma h} \tag{16}$$

This has the general solution

$$f(\vec{u}) = \Re\left[g(u_x + \imath u_y)\right] - \frac{pa^2}{4\gamma h}\left(u_x^2 + u_y^2\right) \tag{17}$$

where $g(\zeta)$ is any analytic function. The simplest solution, given that we want the maximum of (17) to be unity, is to set $g(\zeta) = 1$, which results in the droplet having the shape of the cap of a spheroid. As noted in Berry (1976), however, the far field of such a droplet does not show any catastrophes, and in any case is not a realistic model, because the liquid droplet will never be perfectly smooth. We will explore another choice of $g(\zeta)$ in section 4 when we show the results of numerical simulations of the far field irradiance pattern. A more complete analysis would necesarily invove a discussion of wetting and sessile drops, and it is in principle possible to derive relationships between γ, h, a, and p for a given volume of water, but this is outside the scope of this work. See Zhang et. al. (2005) for an example of catastrophe optics applied to the study of the wetting of liquid drops on a solid surface.

3 Experimental Set-Up

3.1 Equipment

- Distilled water.
- HeNe laser ($\lambda = 632.8$ nm), with power comparable to that of a Melles Griot 05-LHR-321. The refractive index of water is well known ($n = 1.33$) for the wavelength of a HeNe laser, and the relatively low power is essential in order to prevent the water from heating up and evaporating rapidly.
- Circular plate made of thin glass. Should be relatively dirty, otherwise the contact angle between the water and the glass will be too small and the water will spread out and adopt a flat profile.
- Pipette.
- 100 μm pinhole.
- Two 2.5 mm convex lenses. The first will be used to focus the beam into a pinhole, whereas the second one is used to collimate the beam. We don't want the size of the spot at the droplet to be large since the size of the droplet will be very small, and we want the beam to diverge relatively quickly so as to be able to obtain a large enough image at the screen without having to make d too large. This explains why we use a lens with small focal length in order to collimate the light.
- Post holders.
- Beam stopper.
- Vertical breadboard table.
- Translation stage.
- Claw.

3.2 Setup and procedure

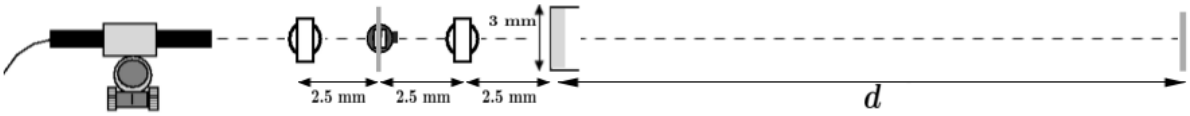

Figure 3: Rotated setup for the experiment. Not to scale. Device figures adapted from Bodenschatz et. al. (2016).

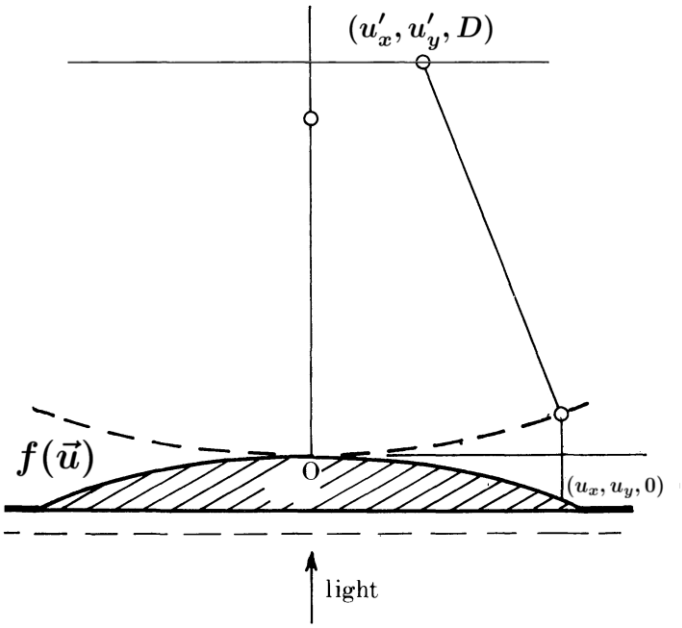

Figure 4: Vertical view of the refraction of the rays as they pass through the lens. Not to scale. Adapted from Nye (1978).

Since the effect of gravity on the droplet is important, the setup of this experiment is vertical, which means that the breadboard table to be used must be set up vertically. A horizontal representation of the setup is shown in Figure 3. We start by mounting the laser, and placing a 2.5 mm lens some small distance away from it. We align the lens such that the reflected beam comes back to its origin at the laser. We now place the pinhole 2.5 mm away from the first lens, and place another convex lens 2.5 mm away from the pinhole, aligned such that the beam goes back onto itself. Next, we mount the claw 2.5 mm away from the second lens and use it to hold the empty plate. We now use the pipette to place a drop of water in the glass. The claw is aligned such that the glass is as perpendicular as possible with respect to the incident light. Finally, we mount the beam stopper in a translation stage a distance $d \gg a$ away from the plate, and translate it towards and away from the plate in order to observe the different types of catastrophes that form at the screen.

3.3 Difficulties and sources of error

The most significant source of error in this experiment is the alignment of the plate with respect to the direction of the incoming light. The plate must be parallel to the floor. If this is not the case, gravity will deform the drop and equation (19) will not describe its shape. Furthermore, the light will no longer be incident normally with respect to the drop, which adds another term to the lens equation. Finally, any deviation from the parallel position will result in the light to be refracted by the glass that makes up the bottom surface of the plate, and the lensing will no longer be due to the droplet only. This alignment will be made harder by the fact that the water volume needs to be very small: for a drop with $h = 0.5$ mm and characteristic radius $a = 1.5$ mm, the volume of the drop is $\sim 1.2\,\mu$L, which is about $1/50$ of the volume of a standard drop. Thus, it might prove hard to make the laser

beam pass through the droplet.

Another important source of error is the drop's evaporation. Since the amount of water involved is minuscule, it will not take long for the water to evaporate, especially considering that laser light is incident on it. This means that the water level at the plate must be monitored and a new drop should be added every few minutes.

4 Expected results

4.1 Simulations

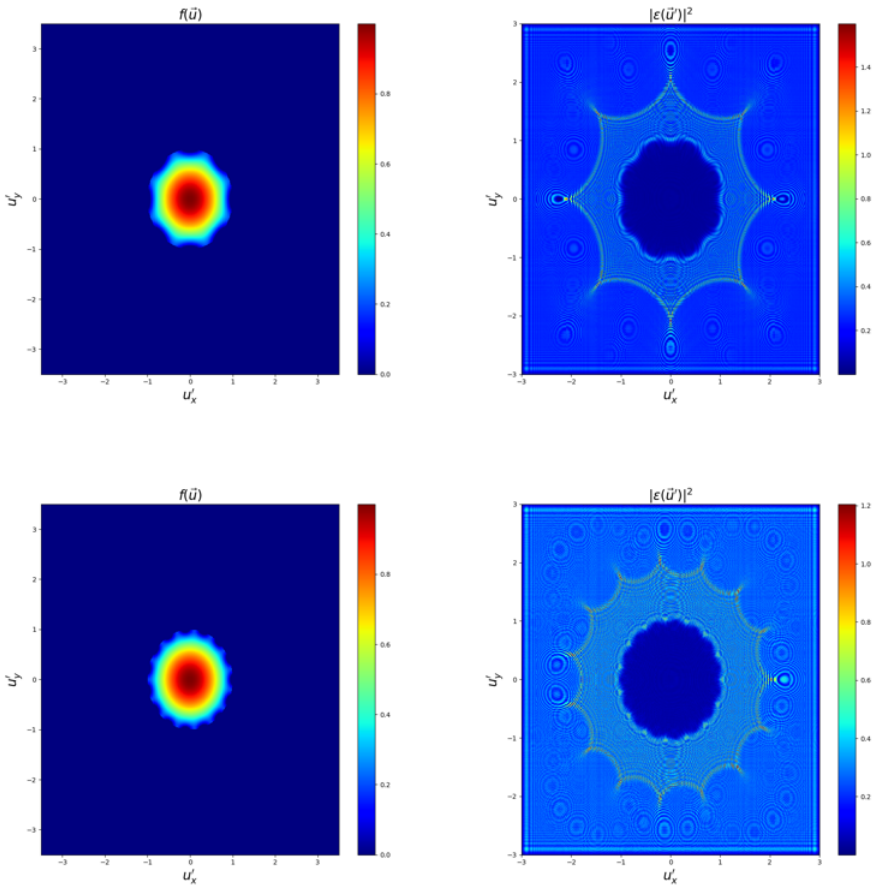

Figure 5: Simulations using the model given in (18). For the top panel $m = 8$, whereas for the bottom panel $m = 15$. The magnitude of the perturbation in both cases is $c = 0.3$, $d = 60$ mm, and $h = 0.5$ mm.

For simulation purposes, we simplify equation (17) by setting $\frac{pa^2}{4\gamma h} = 1$. With $a = 1.5$ mm, $h = 0.5$ mm, and $\gamma = 0.0728$ Nm^{-1}, this gives a value for $p \approx 64.7$ Pa, which is a reasonable value for the internal pressure of a water droplet. Following Berry (1976), we choose $g(\zeta) = 1 - c\zeta^m$, where c is a parameter that determines the deviation of the water droplet from a paraboloid shape. With these two choices, (17) becomes

$$f(\vec{u}) = 1 - \Re\left[c(u_x + \imath u_y)^m\right] - u_x^2 - u_y^2 \tag{18}$$

We note that the diffraction integral (12) is a convolution integral of the functions

$$\begin{aligned} J(\vec{u}) &= \exp\left[\imath kh(1-n)f(\vec{u})\right] \\ K(\vec{u}') &= \frac{1}{2\pi u_F^2} \exp\left[\frac{\imath\,|\vec{u}'|^2}{2u_F^2}\right] \end{aligned} \tag{19}$$

This means that in principle, we can numerically solve the integral using the convolution theorem. Although some aliasing effects are present, we were able to carry out some successful simulations with the choices of $m = 8$ and $m = 15$, and $c = 0.3$. These are shown in Figure 5. Fold and cusp catastrophes are clearly visible, and the caustics form a hypocycloid with m cusps, as expected based on the discussion in Berry (1976). Higher order catastrophes could not be reproduced using this simple choice of $g(\zeta)$, but more convoluted contours should render them visible, as shown in the next section. Figure 6 shows a magnified cusp catastrophe, obtained from the top panel of Figure 5, which shows a structure that is consistent with expectations.

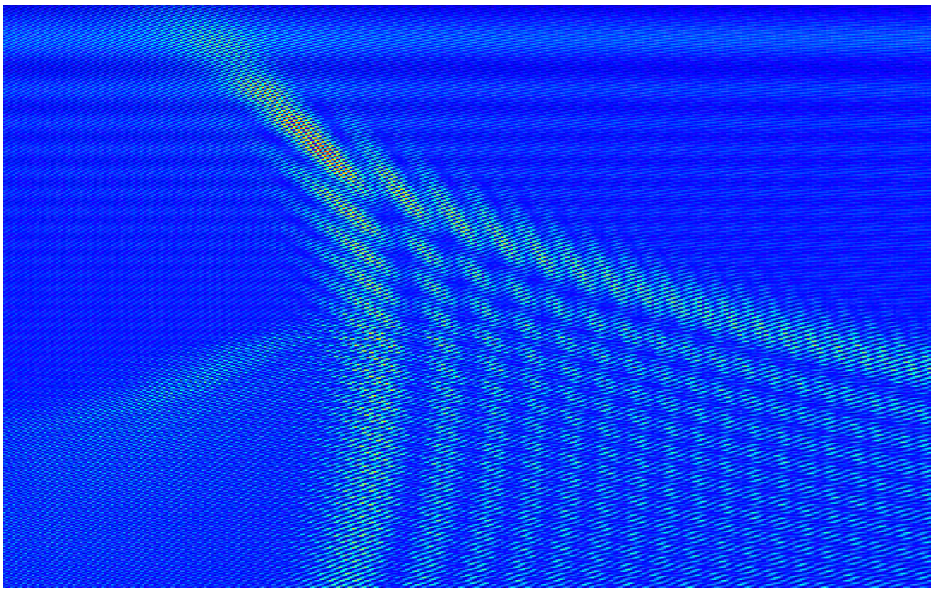

Figure 6: Magnified image of one of the cusps from the top panel of Figure 5.

4.2 Results from similar experiments

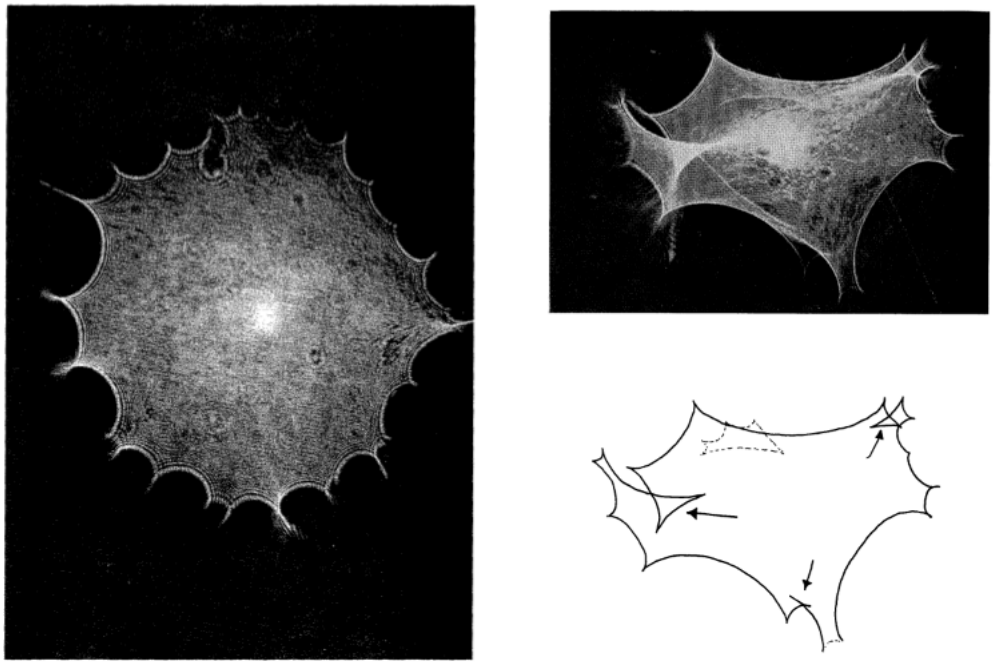

Figure 7: Experimental photographs of far field patterns of small irregular water droplets. The bottom right drawing shows the location of swallowtail catastrophes in the picture above. Adapted from Berry (1976).

Berry (1976) contains a few examples of far field patterns that were obtained experimentally, two of which are shown in Figure 7. The left picture is very similar to the pattern obtained in the simulations of the previous section, only with a larger parameter m. As in the simulations, only folds and cusps are visible. The picture on the right, on the other hand, shows the pattern of a comparatively more irregular shape, and it is possible to observe swallowtails, whose locations are indicated in the drawing below the picture. It is in principle possible to observe higher order catastrophes depending on the shape of the droplet; however, there is significant uncertainty about whether this will be possible in any given experiment, since this will depend on the specific shape that the droplet adopts, which is not something that can be controlled precisely by the experimenter.

Other similar experiments include Nye (1978), where a microscope is used to study the caustics in the near field, and Nye (1986), which studies larger water droplets where gravity is no longer negligible. He is able to produce catastrophes of higher order than those obtained by Berry (1976).

5 Conclusions

Although largely ignored by most traditional textbooks in optics and electromagnetic theory, catastrophe optics is an important area of the field that has found applications in multiple physical disciplines. The purpose of this project was to present the basic ideas behind it, and to show a simple experiment

that could be used to illustrate them. We have performed some simulations of the possible results of the experiment for a simplified model of a water droplet, found that it is possible to numerically reproduce some low order catastrophes using this approach, and that the model is surprisingly accurate when compared to the results of actual experimental work. A more sophisticated approach would likely perform even better. More complex experiments can be devised as a straightforward extensions to the one presented here, by increasing the size of the water droplet, exploring the near field pattern with a microscope, using other liquids, placing the droplets on other types of transparent surfaces, and orienting the surface at an angle with respect to the floor.

References

[1] Arnol'd, V. I., 1975. Russ. Math. Survs. 30, 1-75.

[2] Berry, M. V. 1976. Adv. Phys. 25, 1-26.

[3] Berry, M., & Upstill, C. 1980, in Progress in Optics, Vol. 18, {IV} Catastrophe Optics: Morphologies of Caustics and Their Diffraction Patterns, ed. E. Wolf (Elsevier), 257-346.

[4] Bodenschatz, E., et al., 2016. *Modern Experimental Optics Laboratory Manual*, Cornell University Physics Department.

[5] Born, M. & Wolf, E. 1999. *Principles of Optics, 7th (expanded) edit.,* Cambridge University Press.

[6] Clegg, A. W., Fey, A. L., & Lazio, T. J. W. 1998, ApJ, 496, 253-266.

[7] Cordes, J. M., Wasserman, I., Hessels, J. W. T., et al. 2017, ApJ, 842, 35-45.

[8] Nye, J. F., 1978, Proc. R. Soc. Lond. 361, 1704, 25-44.

[9] Nye, J. F., 1986, Proc. R. Soc. Lond. 403, 1824, 1-26.

[10] Thom, R., 1972. *Stabilité structurelle et morphogénèse.* Benjamin, Reading, Mass.

[11] Thorne, K. & Blandford, R. 2017. *Modern Classical Physics.* Princeton University Press.

[12] Zhang, N., Chao, D. F., Yang, W.-J., 2005. Journal of Flow Visualization & Image Processing. 12, 285-300.